A novel structural design for force/torque fingertip sensors

1998 Meas. Sci. Technol. 9 1196

(http://iopscience.iop.org/0957-0233/9/8/009)

Meas. Sci. Technol. **9** (1998) 1196–1203. Printed in the UK PII: S0957-0233(98)86918-X

A novel structural design for force/torque fingertip sensors

Ying-Hwi Chang†, Yu-Chung Huang†, Yung-Ping Liu‡ and Shyh-Maw Tsay‡

† Institute of Electronics, National Chiao Tung University§, 1001 Ta Hsueh Rd, Hsinchu, Taiwan, Republic of China
‡ Precision Instrument Development Center National Science Council, The Executive Yuan 20 R&D Rd IV, Hsinchu Science-Based Industrial Park, Hsinchu, Taiwan, Republic of China

Received 18 August 1997, in final form 27 January 1998, accepted for publication 27 March 1998

Abstract. This work presents a novel structural design of force/torque fingertip sensors for sensing planar forces. The resolution can be increased by reducing the condition number of the calibration matrix and the sensitivity can be enhanced by placing strain gauges at specified positions. Moreover, the interaction from off-axis loads is intrinsically negligible in our design. A relatively simple and accurate calibration method for performance evaluation is introduced. Some experimental results are presented to demonstrate the capability of the proposed design.

Keywords: sensor, force sensor, force/torque sensor, conditioner number

1. Introduction

Fingertip sensors can provide relevant information, e.g. contact forces and contact locations, to enable robots to perform dextrous manipulation and haptic perception. Robotics research has classified fingertip sensors as either tactile array 'extrinsic' sensing, or 'intrinsic' contact sensing [1–6]. In this work, we are concerned with intrinsic or force/torque fingertip sensors. These sensors are composed of a mechanical structure (a 'body') and several sensing elements placed at specified locations of the body to measure stress. According to the hard finger model [3], the relationship between the measured stress vector and actual forces (as well as torques) can be expressed as a linear system as indicated by equation (1)

$$\boldsymbol{F} = \mathbf{C} \cdot \boldsymbol{V} \tag{1}$$

where $\boldsymbol{F}$ denotes the measured force vector, $\boldsymbol{V}$ represents the measured stress vector and $\mathbf{C}$ is the calibration matrix. $\boldsymbol{F}$ is therefore calculated from $\boldsymbol{V}$ and other contact information can then be derived from $\boldsymbol{F}$ and the geometrical description. Interference in either $\mathbf{C}$ or $\boldsymbol{V}$ owing to the measurement uncertainty can cause significant errors in $\boldsymbol{F}$ [7].

By checking the degree of the relative errors mentioned above, three approaches can be adopted to increase the accuracy. The first approach attempts to search for a more accurate calibration matrix [8–10]. Many errors related to the intrinsic sensing method can be traced to inaccurate calibration [11]. The second approach aims to reduce the error while measuring stress. To do so, extremely precise and expensive electronic instruments are necessary. The third approach aims to increase the resolution of the sensors by reducing the condition number of calibration matrix. For a six-axial fingertip sensor, its condition number of its calibration matrix can be reduced to 4.2 [5]. The condition number of the calibration matrix for a three-axial fingertip force sensor can be as large as 20.05 [11].

In this work we present a novel structure for force/torque fingertip sensors used for sensing planar forces. The proposed design is optimized to increase its resolution and sensitivity. The resolution is enhanced by reducing the condition number of its calibration matrix. This can be reduced, theoretically and experimentally, to 2.55 and 3.34 respectively, i.e. markedly less than the 20.05 found previously [11]. In addition, the sensitivity can be maximized since the transducers are designed to be placed at the most stress-sensitive points. The rest of this paper is organized as follows. Section 2 presents the sensor structure and its theoretical analysis. Section 3 introduces an optimization procedure to determine the sensor's dimensions and adequate locations for the strain gauges. Section 4 presents some experimental results to demonstrate our design. Concluding remarks are finally made in section 5.

2. Structure and analysis

As figure 1 depicts, our proposed design comprises a hemispherical fingertip, two beams with the vertical one

§ Tel: +886 3 5712121 ext 54208. Fax: +886 3 5724361. E-mail address: u7911505@cc.nctu.edu.tw

0957-0233/98/081196+08$19.50

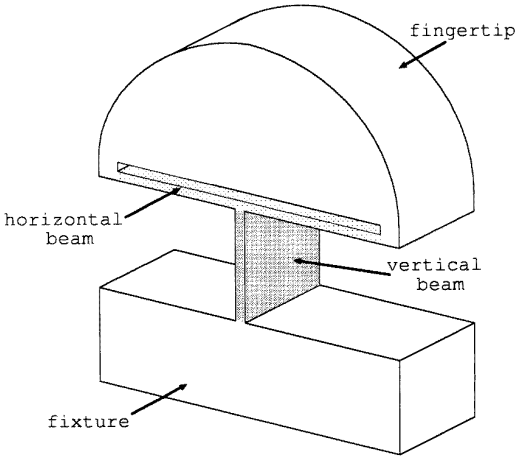

Figure 1. The proposed fingertip sensor in isotropic view.

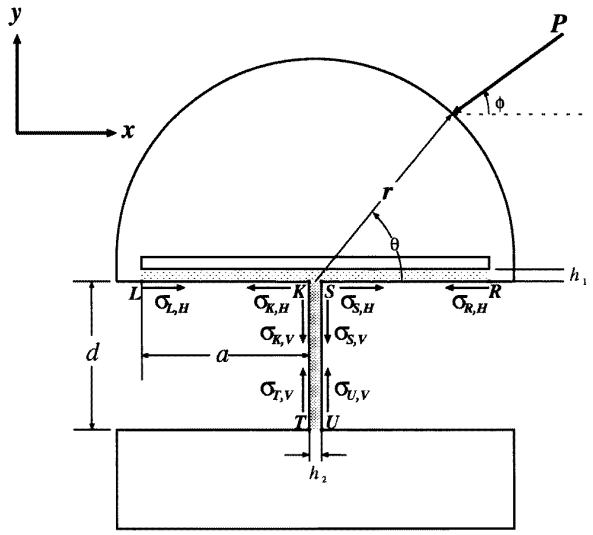

Figure 2. Fingertip sensor cross section view.

propping up the horizontal one, and a fixture. The fingertip guides the applied force to bend the beams. Most of the bending occurs on the beams because they are much thinner than either the fixture or the fingertip. The fixture is attached to the other end of the vertical beam and this provides a structure for the reactive force and torque to balance the applied force. In addition, the beams are sensitively bent by planar forces. The thickness and length of the two beams can be designed to satisfy the requirements for size, sensitivity and dynamic range. The sensor operates in a plane, accounting for why the cylindrical fingertip is oriented to form a hemispherical cross section in this plane and the applied force is reduced to an average force in the plane, as indicated in figure 2. The contact information, i.e. the magnitude of the applied force P, the direction of the applied force ϕ and the contact angle θ can be derived by measuring the beam stresses. The points L, R, T, U, K and S at the fixed ends and joints of both beams are stress-sensitive. Therefore, the stresses at these points (when a force load is applied to the structure) are useful for optimization. Moreover, the analysis of two-dimensional rectangular beams [12] can also be used.

The fingertip and the fixture are simplified in the analysis because their bending is markedly less than that of the beams. For simplicity, the relations between the x-direction component of the applied force and the stresses at the points L, R, T, U, K and S are also considered here. As figure 3 indicates, the structure is reduced to two equivalent structures for analysing the surface stresses of the horizontal and vertical beams while considering only the x-direction force acting on the fingertip. The equivalent force P_x equals $P\cos\phi$. In addition, the equivalent moment M_x, as shown in equation (2), is generated by the x-direction component of the applied force with the pivot at the horizontal beam's centre.

$$M_x = P_x r \sin\theta. \tag{2}$$

Figure 3(a) displays the equivalent structure for deriving the stress along the horizontal beam. Therefore, the stress at the point L along the horizontal beam due to the x-direction component of the applied force is found by

$$\sigma_{Lx,H} = -\frac{3}{2}\frac{M_x}{h_1^2} - \frac{P_x}{2}\frac{1}{h_1} \tag{3}$$

where the other parameters are defined in figure 2.

The stress at point K due to the x-direction component of the applied force along the horizontal beam can be found from

$$\sigma_{Kx,H} = 3\frac{M_x}{h_1^2} - \frac{P_x}{2}\frac{1}{h_1}. \tag{4}$$

The structure in figure 3(b) is used to analyse the stress along the vertical beam. The bending moments at the TU and KS cross sections are expressed, respectively, as

$$M_{TUx,V} = -P_x(d + r\sin\theta + h_1/2) \tag{5}$$

$$M_{KSx,V} = -P_x(r\sin\theta + h_1/2). \tag{6}$$

In addition, the stresses at point T and K along the vertical beam due to the bending of the vertical beam by the x-direction force are derived from

$$\sigma_{Tx,V} = \frac{6}{h_2^2}M_{TUx,V} \tag{7}$$

$$\sigma_{Kx,V} = \frac{6}{h_2^2}M_{KSx,V}. \tag{8}$$

Owing to geometrical symmetry with respect to the y-axis, the stresses at point U, S and R from the x-direction component of the applied force are negative to their symmetrical points T, K and L. Restated, the stresses $\sigma_{Rx,H}$, $\sigma_{Sx,H}$, $\sigma_{Ux,V}$ and $\sigma_{Sx,V}$ are negative to $\sigma_{Lx,H}$, $\sigma_{Kx,H}$, $\sigma_{Tx,V}$ and $\sigma_{Kx,V}$ respectively.

On the other hand, while considering only the y-direction component of the applied force acting on the fingertip, figure 4 displays equivalent structures for analysing the surface stresses of both beams. The equivalent force P_y equals $P\sin\phi$, which is the y-direction component of the applied force. The equivalent moment

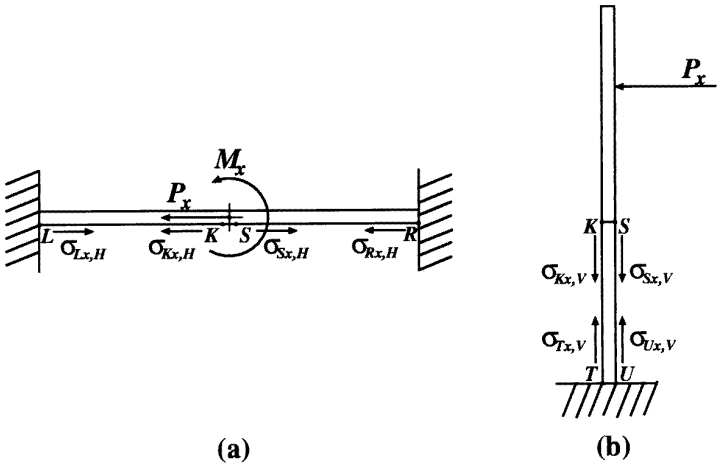

Figure 3. The equivalent structures when considering only the *x*-direction component of the applied force for analysing the surface stress along (*a*) the horizontal beam and (*b*) the vertical beam.

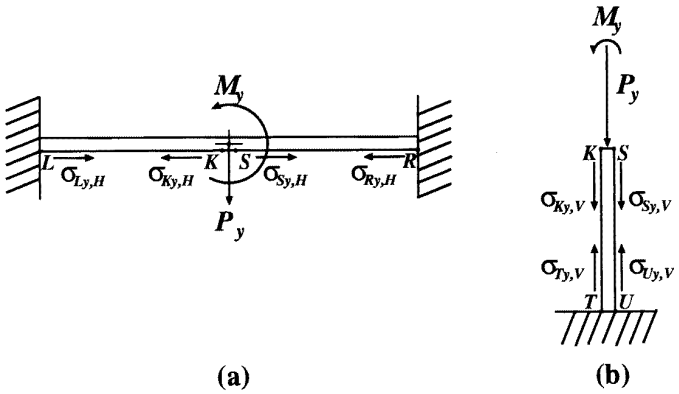

Figure 4. The equivalent structures while considering only the *y*-direction component of the applied force for analysing the surface stress along (*a*) the horizontal beam and (*b*) the vertical beam.

M_y, as shown in equation (9), is induced by the y-direction component of the applied force with the pivot on the symmetrical axis:

$$M_y = -P_y r \cos\theta. \tag{9}$$

Figure 4(*a*) presents the equivalent structure for analysing the stress along the horizontal beam. The stress at point L along the horizontal beam due to the y-direction component of the applied force is

$$\sigma_{Ly,H} = -\frac{3}{2}\frac{P_y a}{h_1^2} - \frac{3}{2}\frac{M_y}{h_1^2} \tag{10}$$

and the stress at point K along the horizontal beam due to the y-direction component of the applied force is

$$\sigma_{Ky,H} = \frac{3}{2}\frac{P_y a}{h_1^2} + 3\frac{M_y}{h_1^2}. \tag{11}$$

The structure in figure 4(*b*) is used to derive the stress along the vertical beam. The stresses at points T and K along the vertical beam due to the y-direction force are

$$\sigma_{Ty,V} = -\frac{6}{h_2^2}M_y - \frac{P_y}{h_2} = \sigma_{Ky,V}. \tag{12}$$

According to our results, the equivalent force exerted the same effect on both sides around the structure's symmetrical axis. In addition, the equivalent moment has contradictory effects on both sides around the symmetrical axis. Therefore, the stresses at points R, S and U from the y-direction component of the applied force can be derived by modifying the stresses at their symmetrical points L, K and T as shown by equations (13)–(15):

$$\sigma_{Ry,H} = -\frac{3}{2}\frac{P_y a}{h_1^2} + \frac{3}{2}\frac{M_y}{h_1^2} \tag{13}$$

$$\sigma_{Sy,H} = \frac{3}{2}\frac{P_y a}{h_1^2} - 3\frac{M_y}{h_1^2} \tag{14}$$

$$\sigma_{Uy,V} = \frac{6}{h_2^2}M_y - \frac{P_y}{h_2} = \sigma_{Sy,V}. \tag{15}$$

The stress at each end of the beam can be found by taking the superposition of the individual stress component obtained previously. Table 1 summarizes the stresses at points L, R, T, U, K and S by the applied force on the finger tip. By applying the results in table 1 and according to the hard finger model of equation (1), the force vector

Table 1. Summary of the stresses at points L, R, T, U, K and S of the proposed structure in the form: $\sigma = P(g_1 \sin\phi + g_2 \sin(\phi - \theta) + g_3 \cos\phi)$.

Name of stress	Components	g_1	g_2	g_3
$\sigma_{L,H}$	$\sigma_{Lx,H}\sigma_{Ly,H}$	$-\frac{3}{2}\frac{a}{h_1^2}$	$\frac{3}{2}\frac{r}{h_1^2}$	$-\frac{1}{2h_1}$
$\sigma_{R,H}$	$\sigma_{Rx,H}\sigma_{Ry,H}$	$-\frac{3}{2}\frac{a}{h_1^2}$	$-\frac{3}{2}\frac{r}{h_1^2}$	$\frac{1}{2h_1}$
$\sigma_{T,V}$	$\sigma_{Tx,V}\sigma_{Ty,V}$	$-\frac{1}{h_2}$	$\frac{6r}{h_2^2}$	$-\frac{6}{h_2^2}(d + \frac{h_1}{2})$
$\sigma_{U,V}$	$\sigma_{Ux,V}\sigma_{Uy,V}$	$-\frac{1}{h_2}$	$-\frac{6r}{h_2^2}$	$\frac{6}{h_2^2}(d + \frac{h_1}{2})$
$\sigma_{K,H}$	$\sigma_{Kx,H}\sigma_{Ky,H}$	$\frac{3}{2}\frac{a}{h_1^2}$	$-\frac{3r}{h_1^2}$	$-\frac{1}{2h_1}$
$\sigma_{S,H}$	$\sigma_{Sx,H}\sigma_{Sy,H}$	$\frac{3}{2}\frac{a}{h_1^2}$	$\frac{3r}{h_1^2}$	$\frac{1}{2h_1}$
$\sigma_{K,V}$	$\sigma_{Kx,V}\sigma_{Ky,V}$	$-\frac{1}{h_2}$	$\frac{6r}{h_2^2}$	$-\frac{3h_1}{h_2^2}$
$\sigma_{S,V}$	$\sigma_{Sx,V}\sigma_{Sy,V}$	$-\frac{1}{h_2}$	$-\frac{6r}{h_2^2}$	$\frac{3h_1}{h_2^2}$

Table 2. Summary of the stresses at points L, R, T, U, K and S of the proposed structure with $a = d = r$.

Name of stress	θ	ϕ	Maximum stress	Maximum stress for $h_2 = 1.633h_1$
$\sigma_{L,H}$	180°	90°	$3\frac{a}{h_1^2}P$	$3\frac{a}{h_1^2}P$
$\sigma_{R,H}$	180°	−90°	$3\frac{a}{h_1^2}P$	$3\frac{a}{h_1^2}P$
$\sigma_{T,V}$	0°	90°	$12\frac{a}{h_1^2}P$	$4.5\frac{a}{h_1^2}P$
$\sigma_{U,V}$	0°	−90°	$12\frac{a}{h_1^2}P$	$4.5\frac{a}{h_1^2}P$
$\sigma_{K,H}$	180°	90°	$4.5\frac{a}{h_1^2}P$	$4.5\frac{a}{h_1^2}P$
$\sigma_{S,H}$	0°	90°	$4.5\frac{a}{h_1^2}P$	$4.5\frac{a}{h_1^2}P$
$\sigma_{K,V}$	0°	90°	$6\frac{a}{h_1^2}P$	$2.25\frac{a}{h_1^2}P$
$\sigma_{S,V}$	0°	−90°	$6\frac{a}{h_1^2}P$	$2.25\frac{a}{h_1^2}P$

Table 3. Condition number list for the smallest three cases with $h_2 = 1.633h_1$ from theoretical analysis, simulation and measurement.

Case	Stress to measure	Theory	Simulation	Measurement
I	$\sigma_{K,H}\sigma_{S,H}\sigma_{U,V}$	2.55	2.53	3.50
II	$\sigma_{L,H}\sigma_{S,H}\sigma_{U,V}$	2.62	3.36	3.50
III	$\sigma_{L,H}\sigma_{R,H}\sigma_{U,V}$	2.69	3.94	3.34

and the stress vector to be measured for the sensors are

$$\boldsymbol{F} = [P\sin\phi \;\; P\sin(\phi - \theta) \;\; P\cos\phi]^{\mathrm{T}} \tag{16}$$

$$\boldsymbol{V} = [\sigma_1 \;\; \sigma_2 \;\; \sigma_3]^{\mathrm{T}} \tag{17}$$

where σ_1, σ_2 and σ_3 are different stresses chosen from table 1. Then the theoretical calibration matrix can be formed from the corresponding coefficients listed in table 1.

3. Design optimization

The following steps describe how to optimize the proposed structure with respect to the sensitivity and resolution.

3.1. Equalizing the maximum stress on each beam

Reducing the variation of the stresses measured for the two thin beams facilitates an increase in the sensitivity and a decrease in the condition number of the calibration matrix. This reduction can be achieved by dimensioning the structure such that the maximum stresses on the two beams are equal. The constraints on the structure's dimensions come primarily from the limitation of fabrication procedures, particularly from the glueing of strain gauges. Hence, the length of the horizontal beam a and the length of the vertical beam d are set equal and adjusted together to satisfy the space requirements while glueing strain gauges. Table 2 summarizes the maximum stresses at points L, R, T, U, K and S with $a = d = r$. As figure 2 depicts, r should be slightly larger than a; however, this does not significantly affect the optimized results. As observed herein, the maximum stress for the horizontal beam is $\sigma_{K,H}$ for $\theta = 180°$ and $\phi = 90°$, and $\sigma_{S,H}$ for $\theta = 0°$ and $\phi = 90°$. The maximum stress for the vertical beam is $\sigma_{T,V}$ for $\theta = 0°$ and $\phi = 90°$, and

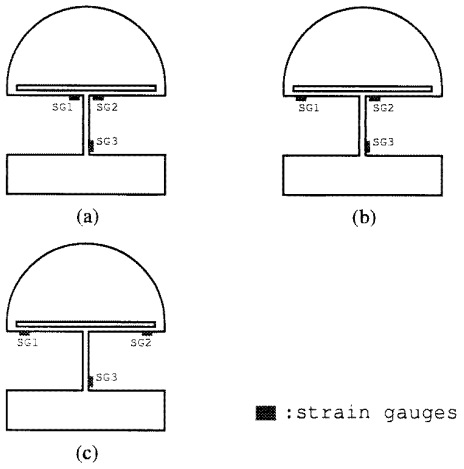

Figure 5. The three cases for the placement of strain gauges: (*a*) case I; (*b*) case II; (*c*) case III.

$\sigma_{U,V}$ for $\theta = 0^\circ$ and $\phi = -90^\circ$. According to table 2, the maximum stresses on both beams can be equalized by setting $h_2 = 1.633h_1$. In summary, points K and S are the most stress-sensitive for the horizontal beam and the most stress-sensitive points for the vertical beam are points T and U.

3.2. Minimizing the condition number of the calibration matrix

The term condition number denotes an important index to characterize the ability of a linear system to resist external interferences [7]. The accuracy of the solved vector space is nearly inversely proportional to the condition number. With reference to equation (1), the noise in the measured stress vector $\boldsymbol{V}$ and the calibration matrix $\mathbf{C}$ results in magnified noise in the measured force vector $\boldsymbol{F}$ which is about equal to the noises in $\mathbf{C}$ and in $\boldsymbol{V}$ multiplied by the condition number of calibration matrix $\mathbf{C}$ [7]. Reducing the condition number of the calibration matrix can thus increase the performance of force/torque fingertip sensors.

Placing strain gauges near stress-sensitive points L, R, T, U, K and S is an attempt to gain an increase in sensitivity. Simultaneously, our results indicate the minimal condition number of the calibration matrix among the different configurations for the placement of the strain gauges at these points. Figure 5 shows that only three cases have the three minimal condition numbers of the calibration matrix. For the other cases, the condition numbers of the calibration matrix are several times larger than those of the three cases. Therefore, they are not evaluated further here. Table 3 summarizes the results of theoretical derivations against the results of finite-element simulations by ANSYS. As figure 5(*a*) reveals, case I has strain gauges SG1, SG2 and SG3, respectively, placed at K, and S on the horizontal beam and at U on the vertical beam—all are the most stress-sensitive positions in the structure. Therefore, the sensitivity of our proposed structure is intrinsically maximized for this case. Although all the strain gauges for cases II and III are not placed at the most stress-sensitive points, their condition numbers are still very close to those obtained for case I. Hence, cases II and III are viable alternatives to case I. Figure 6 depicts a simulation of the influences on the condition number from the position deviation of the strain gauges along each beam. Nevertheless the three cases are chosen under specific conditions; their condition numbers are very close to the local minimum, as indicated in figure 6. In addition, the

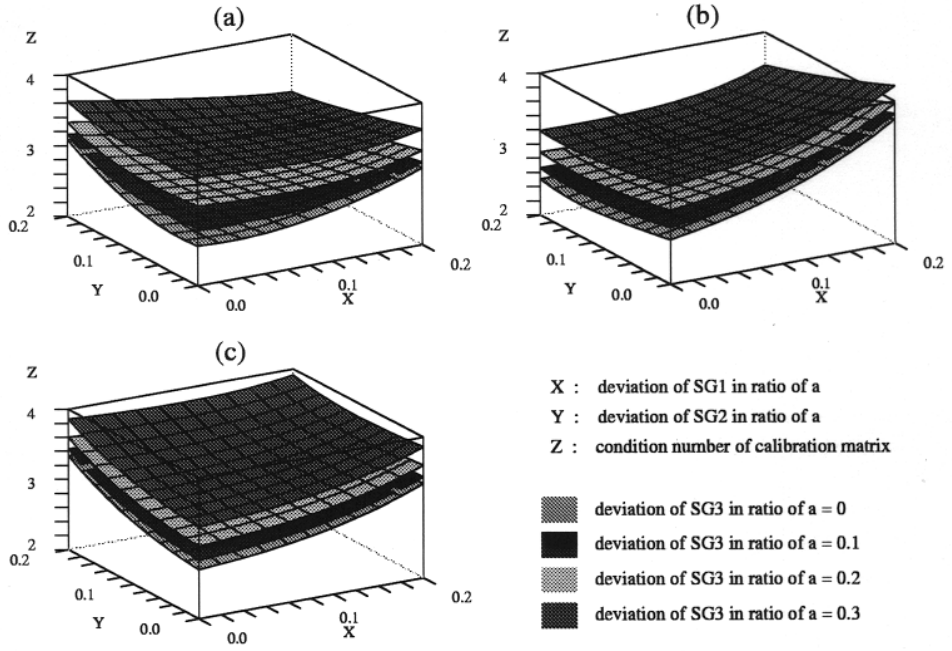

Figure 6. Condition number variation due to position variation of strain transducers for (*a*) case I (*b*) case II and (*c*) case III.

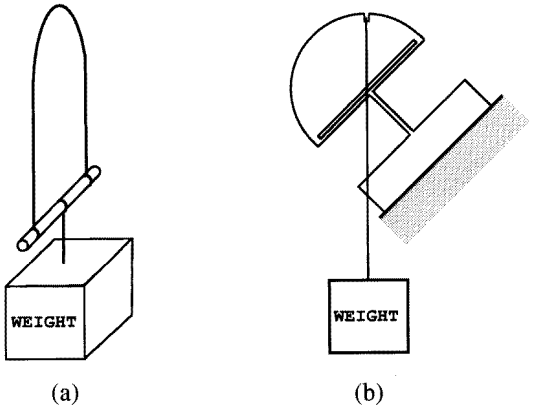

Figure 7. (*a*) Hanging weight and (*b*) applying the weight for calibration.

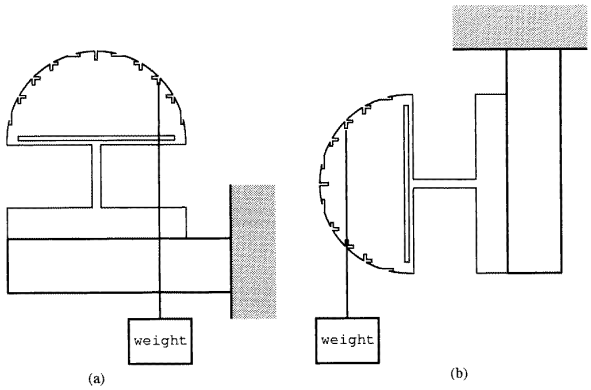

Figure 8. Applied weight at (*a*) $\theta = 45^\circ$, $\phi = 90^\circ$; (*b*) $\theta = 45^\circ$, $\phi = 0^\circ$.

position deviation of SG3 influences the condition number of the calibration matrix more than the position deviations of SG1 and SG2.

3.3. Reducing the interaction from off-axis loads

Off-axis loads generally affect the structure in two aspects. First, although off-axis loads induce the z-direction bending, the large aspect ratio of the thin beams makes this bending insignificant. Second, along each thin beam's direction, off-axis loads produce twisting moments, subsequently invoking a torsion on each beam. Although the shear stresses due to the torsions affect the sensing of strain gauges, this effect is insignificant for the three cases mentioned above because the points L, R, T, U, K and S are on fixed ends for torsions by off-axis loads. Meanwhile, shear stresses by torsion at these points are equal to zero [12].

4. Experimental results

4.1. Calibration method

Using a similar concept to emulate a force load by weight [13], we tied a weight on a rope to the structure, as shown in figure 7(*a*). A groove on the surface of the fingertip allowed the rope to remain fixed, as shown in figure 7(*b*). Applying a specific directional force on the sensor can be achieved by (i) adding a groove starting at the contact point and extending toward the force direction, (ii) aligning the groove direction with the direction of gravity and (iii) hanging the weight in the groove.

At least three kinds of forces are necessary to obtain the calibration matrix. Therefore, for calibration and performance evaluation, we fabricated a structure with x-directional grooves for x-direction forces at $\theta = 5^\circ$, 15°, 30°, 45°, 60°, 120°, 135°, 150°, 165°, 175° and y-directional grooves for y-direction forces at $\theta = 30^\circ$, 45°, 60°, 75°, 90°, 105°, 120°, 135°, 150° (figure 8).

4.2. Sensor fabrication

A force/torque fingertip sensor was designed and fabricated according to the optimization results. We used alloy steel AISI 4340 of 10 mm thickness as a base material and enlarged its plastic range by a thermal process. The structure of the sensor was cut by EDM to dimensions $a = 15$ mm, $b = 15$ mm, $r = 15$ mm, $h_1 = 0.4$ mm and $h_2 = 0.653$ mm. The width of the cutting line was 0.25 mm. Finally, alloy foil strain gauges of gauge length 1 mm were glued onto the structure.

4.3. Measurement results

The resistivity change of the strain gauges was measured by an HP 34401A 6 1/2 digit multimeter. The forces were measured for applying a 4.4 N weight on the grooves between $\theta = 0^\circ$ and $\theta = 90^\circ$. The calibration matrices without scaling for the respective configurations of cases I–III were found by the least-squares method [8], as expressed by the following:

$$\begin{bmatrix} 0.673 & 0.594 & -0.019 \\ -0.280 & 0.238 & 0.002 \\ -0.379 & 0.317 & 0.997 \end{bmatrix}$$

$$\begin{bmatrix} -0.909 & 0.373 & -0.021 \\ 0.377 & 0.349 & 0.003 \\ 0.513 & 0.471 & 1.102 \end{bmatrix}$$

$$\begin{bmatrix} -0.658 & -0.813 & -0.023 \\ 0.608 & -0.755 & -0.011 \\ 0.825 & -1.016 & 1.093 \end{bmatrix}.$$

Their condition numbers were computed at 3.50, 3.50 and 3.34 respectively. According to the simulation results in figure 6, variation of these values from theoretical values could be attributed to the misplacement of the strain gauges from the theoretical positions. The off-axis deviation of the strain gauges profoundly influenced the variation. Figure 9 plots errors in the measurements for diverse loads for case I. Similar error results were also obtained for the other two cases. This degree of error is acceptable for many practical applications.

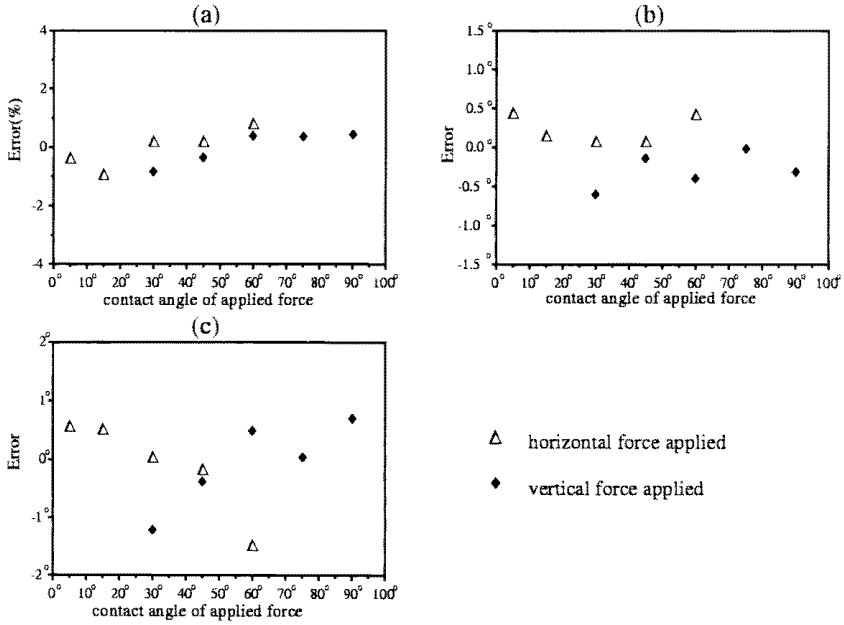

Figure 9. Error plots of force measurements for case I: (*a*) error in force magnitude; (*b*) error in force angle; (*c*) error in contact angle.

5. Conclusions

The sufficient correlation between simulation and experimental results in this work demonstrates the effectiveness of our proposed structure. Sections 2 and 3 provide valuable information for the structural design. Using this information, the condition number of the calibration matrix can be reduced.

It was found that the strain gauges should be placed very close to the most stress-sensitive points for optimal results. Consequently, the resolution and sensitivity of our proposed structure was enhanced. The strain gauge SG3 should be carefully mounted—misplacement of SG3 influences the condition number much more than ill-positioning of SG1 or SG2. The off-axis load, although influencing the torsion effect on thin beams, does not significantly affect the sensing of strain gauges since the strain gauges are mounted at insensitive places for the torsion. Moreover, the structure's dimensions should be considered in advance when glueing strain gauges, thereby reducing the difficulty of mounting. Moreover, the calibration method proposed herein is simple and accurate.

Finally, the proposed structure could be further improved in two respects. First, sizing the sensors down to human fingertip size would require different processes to fabricate miniature structures. Second, reducing the residual bending on the thin beams while glueing and curing the strain gauges could increase the dynamic range of the sensor.

Acknowledgment

The authors thank the National Science Council of the Republic of China for financially supporting this research under the Contract No NSC-842213E009136.

References

[1] Dario P 1991 Tactile sensing: technology and applications *Sens. Actuators* A 251–6
[2] Howe R D 1994 Tactile sensing and control of robotic manipulation *J. Adv. Robot.* **8** (3) 245–61
[3] Salisbury J K 1984 Interpretation of contact geometries from force measurements *Robotics Research* ed M Brady and R Paul (Cambridge, MA: MIT Press) pp 565–77
[4] Salisbury J K 1985 *Robot Hands and the Mechanics of Manipulation* (Cambridge, MA: MIT Press)
[5] Bicchi A and Dario P 1987 Intrinsic tactile sensing for artificial hands *Robotics Research* ed R Bolles and B Roth (Cambridge, MA: MIT Press) pp 83–90
[6] Bicchi A 1990 Intrinsic contact sensing for soft fingers *Proc. Int. Conf. on Robotics and Automation (13–18 May 1990, Cincinnati, OH)* pp 968–73
[7] Maron M J 1982 *Numerical Analysis—A Practical Approach* (London: Macmillan) pp 156–8
[8] Bicchi A and Canepa G 1994 Optimal design of multivariate sensors *Meas. Sci. Technol.* **5** (4) 319–32
[9] Voyles R M *et al* 1995 Shape from motion approach to rapid and precise force/torque sensor calibration *Proc. ASME Dynamic Systems and Control Division, ASME Winter Annual Meeting (San Francisco, CA) November 1995* (New York: ASME) pp 67–73
[10] Voyles R M *et al* 1995 Shape from motion decomposition as a learning approach for autonomous agents *Proc. IEEE Int. Conf. on Systems, Man and Cybernetics (22–25 October 1995, Vancouver)* pp 407–12
[11] Son J S, Cutkosky M R and Howe R D 1996 Comparison of contact sensor localization abilities during manipulation *Robot. Autonom. Systems* **17** 217–33
[12] Pilkey W D 1994 *Formulae for Stress, Strain and Structural Matrices* (New York: Wiley)
[13] Ma D and Hollerbach J M 1996 Identifying mass parameters for gravity compensation and automatic torque sensor calibration *Proc. IEEE Int. Conf. on Robotics and Automation (22–28 April 1996, Minneapolis, MA)* (New York: IEEE) pp 647–54

[14] Zhou X, Shi Q and Li Z 1996 Contact localization using force/torque measurements *Proc. IEEE Int. Conf. on Robotics and Automation (22–28 April 1996, Minneapolis, MA)* (New York: IEEE) pp 1339–44
[15] Tsujimura T and Yabuta T 1989 Object detection by tactile sensing method employing force/torque information *IEEE Trans. Robot. Autom.* **5** (4) 444–50
[16] Voyles R M, Fedder G and Khosla P K 1996 Design of a modular tactile sensor and actuator based on an electrorheological Gel *Proc. IEEE Int. Conf. on Robotics and Automation (22–28 April 1996, Minneapolis, MA)* (New York: IEEE) pp 13–16
[17] Logan D L 1994 *Mechanics of Materials* (New York: Harper Collins)